

# A quantum spin liquid phase in the Kitaev-Hubbard model

Shaojun Dong,<sup>1</sup> Hao Zhang,<sup>2,3</sup> Chao Wang,<sup>1</sup> Meng Zhang,<sup>2,3</sup> Yong-Jian Han,<sup>2,1,3,\*</sup> and Lixin He<sup>2,3,4,†</sup>

<sup>1</sup>*Institute of Artificial Intelligence, Hefei Comprehensive National Science Center*

<sup>2</sup>*CAS Key Laboratory of Quantum Information, University of Science and Technology of China, Hefei 230026, People's Republic of China*

<sup>3</sup>*Synergetic Innovation Center of Quantum Information and Quantum Physics, University of Science and Technology of China, Hefei 230026, China*

<sup>4</sup>*Hefei National Laboratory, University of Science and Technology of China, Hefei 230088, China*

The quantum spin liquid (QSL) state has been searched intensively in Kitaev-like materials, such as the Iridium oxides  $A_2\text{IrO}_3$  and  $\alpha\text{-RuCl}_3$ . The half-filled Kitaev-Hubbard model with bond dependent hopping terms is used to describe the Kitaev-like materials, which is calculated using the state-of-the-art fermionic projected entangled pair states (fPEPS) method. We find a QSL phase near the Mott insulator transition, which has a strong first-order transition to the semi-metal phase with the decrease of Hubbard  $U$ . We suggest that a promising routine to find the QSL is to find the Iridium oxides that are near the Mott insulator transitions.

A quantum spin liquid (QSL) [1–3] state is a quantum state that lacks any long range magnetic order even down to zero temperature. QSLs have nontrivial topological properties that may host exotic excitations with fractional statistics, such as spinons, and visons, etc., which may have important applications in quantum computing[4, 5] and may play a crucial role in high-temperature superconductivity.

The Kitaev model[5] is an exactly solvable model on a 2D honeycomb lattice, which hosts a QSL ground state. Several Iridium oxides  $A_2\text{IrO}_3$ , as well as  $\alpha\text{-RuCl}_3$ , have been proposed to realize the Kitaev QSL [6–14]. These materials have a honeycomb structure and the strong spin-orbit coupling leads to an effective  $j_{\text{eff}}=\frac{1}{2}$  spin model with bond dependent anisotropic exchange interactions[8, 15], which are the essential ingredients of the Kitaev model. In addition to the Kitaev exchange interactions, there are also Heisenberg interactions in these materials [16]. The Kitaev-Heisenberg model has been intensively studied, and it has been shown that the QSL can only survive in a rather small parameter space [16–20]. Indeed,  $\text{Na}_2\text{IrO}_3$  and  $\alpha\text{-RuCl}_3$  were found to have a zigzag antiferromagnetic (AFM) order by resonant X-ray magnetic scattering and inelastic neutron scattering experiments. Tremendous efforts have been made to find the QSL in these materials, and yet no evidence of QSL has been found so far[6, 9, 21, 22]. An important question is that given the extremely small parameter space for the QSL in the Kitaev-Heisenberg model, is it even possible to find the Kitaev QSL in real materials?

The Kitaev-Hubbard model is a more realistic model to describe the Iridium oxides. When the Hubbard  $U$  is small, higher order interactions become important, which may introduce exotic states. The Kitaev-Hubbard model has been studied by mean-field theories [23–25]. It has been shown that there exists a QSL phase in the region of  $t' < t$  when  $U$  is small, where  $t$  and  $t'$  are the isotropic and spin-dependent hopping terms respectively. A further decrease in  $U$  results in a semi-metal (SM) phase. However,

these calculations were based on mean-field approximations [23–25], which need to be examined by more rigorous methods. Furthermore, these studies focus on the  $t' < t$  region, and the phase diagram for  $t' > t$  was missing. Experimentally, the Iridium oxides materials, e.g.,  $\text{Na}_2\text{IrO}_3$  and  $\alpha\text{-RuCl}_3$ , are believed to have strong spin-dependent hopping terms[9, 26–28], and in the  $t' > t$  region.

The projected entangled pair states method (PEPS) [29–34], and its generalization to fermionic systems (fPEPS) [35–39] provide systematically improvable variational wave functions for the many-body problems, which allow more rigorous treatment of the Kitaev-Hubbard model. In this Letter, we apply this recently developed and highly accurate fPEPS method to explore the phase diagram of the half-filled Kitaev-Hubbard model. The results show that the QSL state is absent in the  $t' < t$  region in contrast to previous mean-field results [23–25]. Instead, we find a QSL phase in the  $t' > t$  region when  $U$  is small. We show that the phase transition from the SM phase to the QSL phase is a first-order transition, whereas the QSL-zigzag transition is a continuous transition. Given that the Iridium oxide materials and  $\alpha\text{-RuCl}_3$  are in the  $t' > t$  region, it is possible to find suitable materials that may host the QSL.

The Hubbard-Kitaev model reads,

$$H = \sum_{\langle i,j \rangle_{\alpha,s}} \{ \hat{c}_{i,s}^\dagger (\frac{t + t'\sigma^\alpha}{2}) \hat{c}_{j,s} + H.c. \} + U \sum_i \hat{n}_{i\uparrow} \hat{n}_{i\downarrow}, \quad (1)$$

where  $\hat{c}_{i,s}$  is the annihilation operator that destroys an electron with spin  $s$  at site  $i$ , and  $\hat{n}_{i,s} = \hat{c}_{i,s}^\dagger \hat{c}_{i,s}$  is the number operator.  $\sigma^\alpha$ , with  $\alpha=x, y, z$  are the pauli matrices.  $\langle i, j \rangle_\alpha$  denotes the nearest-neighbor pairs in the three hopping directions of the lattice, as sketched in Fig. 1. The  $t$  and  $U$  terms are the hopping and the on-site Coulomb interaction terms in the normal Hubbard model, whereas the  $t'$  is the spin-dependent hopping due to spin-orbit coupling.

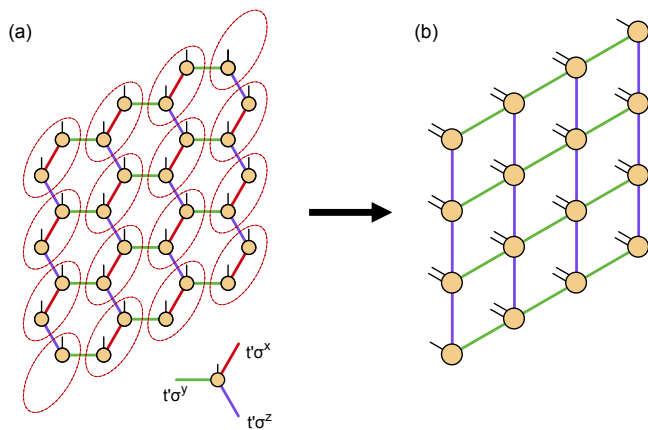


FIG. 1. (Color online) (a) The honeycomb lattice with bond dependent interactions. (b) The honeycomb lattice is mapped to a PEPS defined on a square lattice, where two physical indices on the honeycomb lattice are combined in a single site.

The fPEPS method [29–35] is one of the most promising methods to study strongly correlated electron systems. We simulate the honeycomb lattice with open boundary condition (OBC) using a square tensor network. We map the honeycomb lattice from Fig. 1(a), to a square lattice of Fig. 1(b), where two sites of the honeycomb lattice are treated as a single site in the square lattice (except those sites at the corner, which remain a single site in the square lattice). Each site of tensor network contains two physical indices. The physical properties can still be easily calculated on the physical (honeycomb) lattice. We optimize the wave functions using the so called fPEPS++ method developed in our group [34, 35, 40], i.e., the fPEPS wave functions are optimized via a stochastic gradient method, whereas the energy and energy gradients are calculated using a Monte Carlo sampling method. This method significantly reduces the computational complexity with respect to the bond dimension  $D$ , thereby allowing a much larger bond dimension to be used, resulting in highly accurate and converged results for large finite systems.

All the parameters in the fPEPS wave functions are independent and subject to optimization. We first obtain the quantum wave functions with the simple update method, and the fPEPS wave functions are further optimized using the stochastic gradient method until the results fully converge [34, 35, 40]. In our calculations, the bond dimension  $D=14$  and the truncation bond dimension  $D_c=42$  are used, which show good convergence.

The magnetic phase is determined by the spin structure factor,

$$S(\{\mathbf{k}_\alpha\}) = \sum_{i,j,\alpha} e^{-i\mathbf{k}_\alpha \cdot (\mathbf{r}_i - \mathbf{r}_j)} S_i^\alpha \cdot S_j^\alpha, \quad (2)$$

where  $\mathbf{r}_i$  is the coordinate of the honeycomb lattice and  $S_i^\alpha$  is the spin operator at site  $\mathbf{r}_i$ , with  $\alpha = x, y, z$ . The AFM order is characterized by the non-zero value of the spin structure factor at  $\mathbf{k}_x = \mathbf{k}_y = \mathbf{k}_z = (\frac{4\pi}{3}, 0)$ , whereas the zigzag order is detected by the spin structure at  $\mathbf{k}_x = (\frac{2\pi}{3}, 0)$ ,  $\mathbf{k}_y = (-\frac{\pi}{3}, \frac{\sqrt{3}\pi}{3})$  and  $\mathbf{k}_z = (\frac{\pi}{3}, \frac{\sqrt{3}\pi}{3})$ . The QSL states are distinguished when all these spin orders vanish but still have finite charge gaps,

$$\Delta = E_{N+1} + E_{N-1} - 2E_N, \quad (3)$$

where  $E_N$  is the total energy of the system with  $N$  electrons.

We first discuss the Kitaev-Hubbard model Eq. (1) in the large- $U$  limit. Without loss of generality, we take  $t = 1$  throughout the paper. At half-filling, the model can be reduced to the Kitaev-Heisenberg spin model to the leading order of  $1/U$  [23, 25],

$$H_{\text{eff}} = \sum_{\langle i,j \rangle_\alpha} \left( \frac{1-t'^2}{U} \mathbf{S}_i \cdot \mathbf{S}_j + \frac{2t'^2}{U} S_i^\alpha S_j^\alpha \right), \quad (4)$$

where  $S_i^\alpha$ ,  $\alpha = x, y, z$  are the spin operators at site  $i$  the  $\mathbf{S}_i = (S_i^x, S_i^y, S_i^z)$ , and the  $\langle i, j \rangle_\alpha$  denotes the nearest-neighbor pairs in the three hopping directions of the lattice (see Fig. 1). The Kitaev-Heisenberg model has been studied intensively, and the phase diagram of the model is well known [16, 18, 19, 41–49]. In Ref. 17, the authors extended the original model to its full parameter space, i.e.,

$$H_{\text{KH}} = \sum_{\langle i,j \rangle_\alpha} [J \mathbf{S}_i \cdot \mathbf{S}_j + K S_i^\alpha S_j^\alpha], \quad (5)$$

where  $J = \cos \phi$  is the Heisenberg coupling strength, and  $K = 2\sin \phi$  is the Kitaev coupling strength. The phase angle  $\phi$  may vary from 0 to  $2\pi$ . The phase boundaries have been obtained by exact diagonalization of the Hamiltonian on a 24-site hexagonal lattice with periodic boundary conditions. Compared with the large- $U$  effective Hamiltonian of Eq. 4, the angle  $\phi$  can be related to the  $t'$  as  $\cot \phi = \frac{1-t'^2}{t'^2} > -1$  and  $\sin \phi = \frac{t'^2}{U} > 0$ , and therefore we have a constrain of  $0 \leq \phi < 3\pi/4$  for Eq. 5. In this parameter region, there does exist a QSL phase on  $\phi \in (88^\circ, 92^\circ)$ , corresponding to  $t' \sim (0.99970, 1)$  in Eq. 4, which is almost a single point in the parameter space. It has been shown that when  $t' < 1$ , the ground state is an AFM phase and is the zigzag phase for  $t' > 1$ . Therefore, in the large  $U$  limit, the AFM phase and the zigzag phase are separated by a QSL state that survives (almost) only at the  $t' = 1$  line.

The decrease in  $U$  may introduce higher order spin interactions [23], which may stabilize the QSL phase in a larger region. Several studies have shown some insight into this problem, where the authors claim that an algebraic QSL lies between  $t' \sim 0.7$  and  $t' = 1$ , when  $U$  is small [23–25]. However, these calculations were based

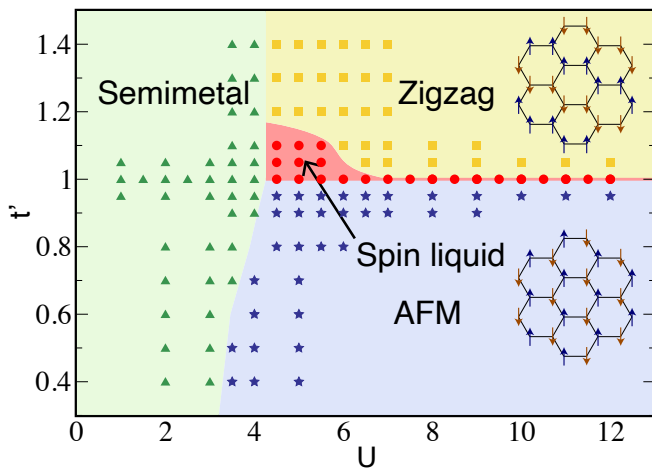


FIG. 2. (Color online) The ground state phase diagram of the Kitaev-Hubbard model on the  $t'$ - $U$  plane, where we have set  $t=1$ . Four phases have been identified including a SM phase, an AFM phase, a zigzag phase and a QSL phase. The scatters represent the parameters that are calculated using the fPEPS method.

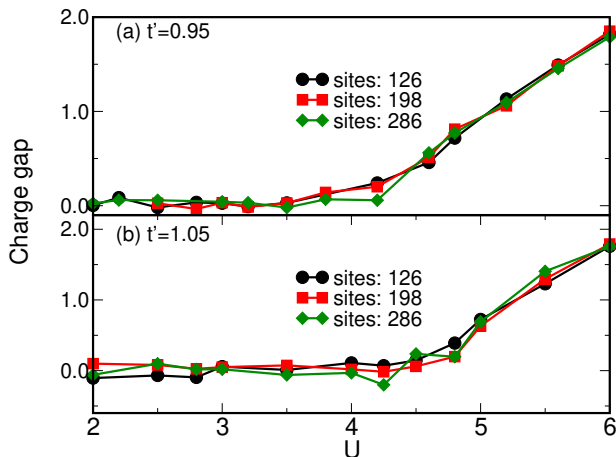


FIG. 3. (Color online) The charge gaps  $\Delta$  on different lattice sizes for (a)  $t' = 0.95$  and (b)  $t' = 1.05$ .

on mean-field approximations [23–25], which need to be examined by more rigorous method. Furthermore, the studies focused on the  $t' < 1$  region, and the phase diagram for  $t' > 1$  was not studied.

We calculate the phase diagram of the Kitaev-Hubbard model in the  $t'$ - $U$  plane, using the fPEPS method, and the results are shown in Fig. 2. Four phases have been identified in the phase diagram. On the left side of the diagram, where  $U$  is small, there is a large SM phase that adiabatically connects to the phase at  $t'=0$ , and  $U=0$ , i.e., the electronic structure of graphene. In the large  $U$  limit, the system is in an AFM phase for  $t' < 1$ , and a zigzag phase, when  $t' > 1$ . Remarkably, there is

a QSL phase in the parameter range  $t' \in (1, 1.2)$  and  $U \in (4.5, 7)$ . For  $U > 7$ , the QSL phase reduces into the  $t'=1$  line, consistent with the results of the Kitaev-Heisenberg model[17].

The SM phase is accompanied by the vanishing of the charge gap. Figure 3(a), (b) depict the charge gaps at  $t'=0.95$  and  $1.05$ , on the honeycomb lattices of 126, 198, 286 sites. The charge gaps decrease with decreasing  $U$ . For both  $t'=0.95$  and  $t'=1.05$ , the charge gaps become zero at approximately  $U \sim 4.5$ , which are the phase boundaries between the SM and Mott insulator phases. The SM phase is further ensured with the vanishing of the local magnetic moment.

We now focus on the insulating region. To determine the magnetic order, we calculate the AFM and zigzag order parameters in the thermodynamic limit via finite size scaling. Figure 4(a), (c) depict AFM and zigzag order parameters for  $U=5$ , with  $t'=0.95, 1, 1.05$  and  $1.2$  as functions of the square root of the number of lattice sites used in the calculations, whereas Fig. 4(b), (d) show the results for  $U=8$ . To reduce the boundary effects, the order parameters are calculated using only the central region of the lattice[34, 40, 50]. For  $U=5$  and  $t'=0.95$ , the system shows a finite AFM order in the thermodynamic limit, and when  $t'=1.2$ , the system shows a zigzag order. However, for  $t'=1$  and  $t'=1.05$ , both AFM and zigzag orders vanish in the thermodynamic limit. In contrast, for  $U=8$  and  $t'=0.95$ , the system also has an AFM order, and for  $t'=1.05$  and  $t'=1.2$ , the system shows a zigzag order. Only when  $t'=1$ , do both AFM and zigzag orders vanish, as expected from the Kitaev-Heisenberg model.[17]

Figure 5(a) depicts the AFM order parameter (in the thermodynamic limit) as a function of  $U$  for  $t'=0.95$ . The AFM order disappears at approximately  $U \sim 4.5$ , which is coincident with the disappearance of the charge gap  $\Delta$ . This result suggests that there is no other phase between the SM and AFM phases. The calculated phase boundary between the SM and AFM phases is in agreement with the mean field results [23–25] for  $t' < 0.8$ . However it shows a distinguishable difference for  $t'$  between 0.8 and 1. Mean field calculations suggest that there is a QSL in this region [23–25], which is absent in more rigorous fPEPS calculations.

Figure 5(b) depicts the AFM and the zigzag order parameters along the line of  $U = 5$ . The system has an AFM order when  $t' < 1$ , and a zigzag order when  $t' > 1.15$ . Both orders disappear in between, which suggests that it is possibly a QSL phase.

To determine the order of the phase transitions, we calculate the first-order energy derivative with respect to  $U$ ,  $\frac{dE}{dU}$ , using the Hellmann-Feynman theorem, i.e.,

$$\frac{dE}{dU} = \langle \Psi | \frac{1}{N} \sum_i \frac{\partial H}{\partial U} | \Psi \rangle = \langle \Psi | \frac{1}{N} \sum_i \hat{n}_{i,\uparrow} \hat{n}_{i,\downarrow} | \Psi \rangle, \quad (6)$$

where  $|\Psi\rangle$  is the ground state fPEPS wave function and  $N$  is the total number of lattice sites that are used to

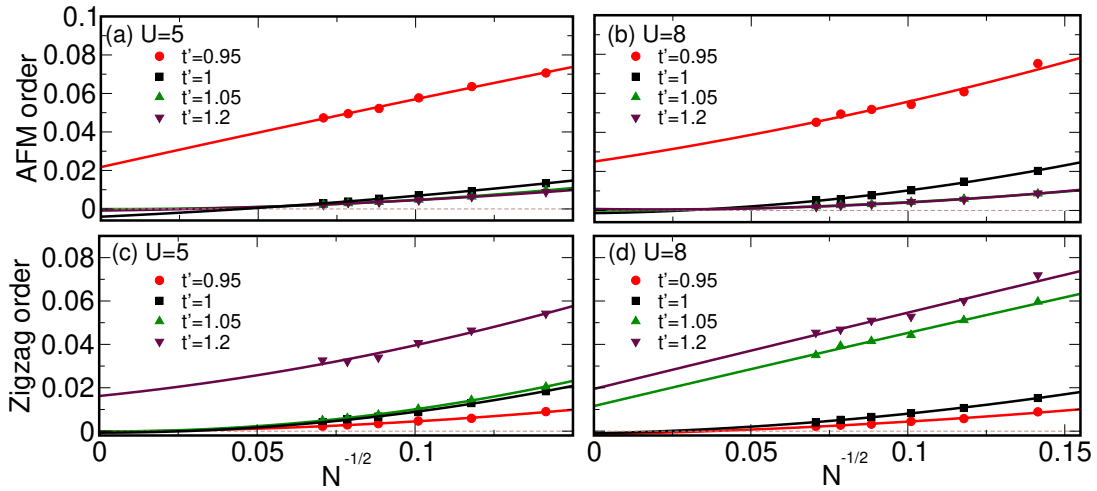


FIG. 4. (Color online) The finite size scaling of the AFM order parameters for (a)  $U=5$  and (b)  $U=8$ . The finite size scaling of the zigzag order parameters is shown in (c) for  $U=5$  and (d) for  $U=8$ .

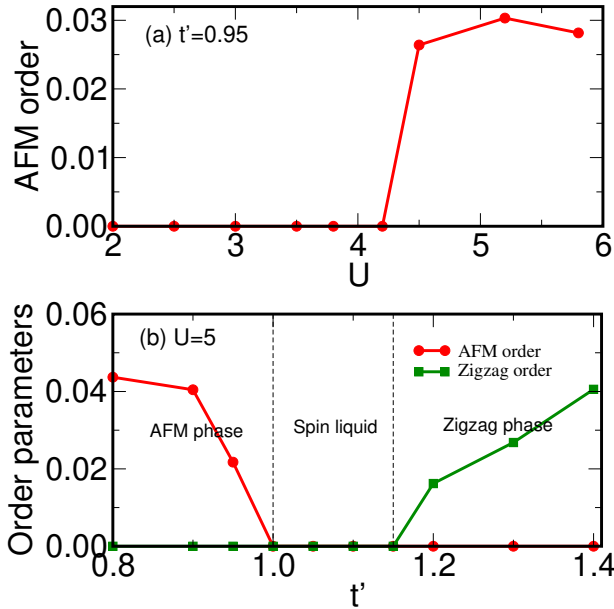


FIG. 5. (Color online) (a) AFM order in the thermodynamics limit as a function of  $U$  for  $t'=0.95$ . (b) AFM order and zigzag order as functions of  $t'$  at  $U=5$ .

calculate the total energy. To reduce the boundary effects, only the central region of lattice is used to calculate the total energies [34, 40, 50]. The results are shown in Fig. 6(a) for  $t'=1.05$ , and the second derivative of the energy with respect to  $U$  (by the finite difference method) are shown in Fig. 6(b). Clearly, there is a sharp discontinuity of  $\frac{dE}{dU}$  at the SM-QSL transition around  $U=4.5$ , which suggests that this is a strong first-order transition. In contrast, the transition between the QSL and zigzag phases is continuous. Note that,  $\langle \hat{n}_{i,\uparrow} \hat{n}_{i,\downarrow} \rangle$  also character-

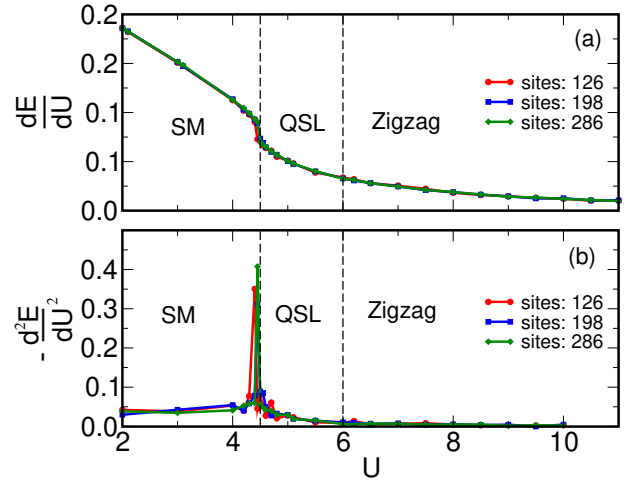


FIG. 6. (Color online) (a) The first-order energy derivative with respect to  $U$  ( $\frac{dE}{dU}$ ), and (b) the second-order energy derivative ( $\frac{d^2E}{dU^2}$ ) on the lattices of different sizes with  $t'=1.05$ .

izes the electron double occupancy on site  $i$ . The QSL-SM transition is driven by the sudden increase of the double occupancy. The QSL phase also benefits from the increase in electron double occupancy.

The values of the Heisenberg coupling  $J$  and the Kitaev coupling  $K$  in real materials, such as  $\text{Na}_2\text{IrO}_3$  and  $\alpha\text{-RuCl}_3$ , have been estimated in Ref.9, 26–28. It has been suggested that in these materials,  $|J| < |K|$  and  $J/K < 0$ , i.e.,  $t' > t$ . We find a large region of zigzag phase in  $\text{Na}_2\text{IrO}_3$  and  $\alpha\text{-RuCl}_3$ , determined by the resonant x-ray magnetic scattering and inelastic neutron scattering experiments[6, 9, 21, 22]. However, since the Iridium oxides are in the  $t' > t$  region, it is a promising routine

to find the QSL in Iridium oxides that are close to the Mott insulator transitions.

To summarize, we calculate the ground state phase diagram of the Kitaev-Hubbard model at half-filling using the recently developed, highly accurate fPEPS method. We obtain the SM phase, AFM phase, and zigzag phase. Remarkably, we find a QSL phase near the Mott insulator transition in the strong bond-dependent hopping region. Our calculations suggest that it is possible to find the QSL in Iridium oxides, which have strong spin-dependent hopping and are close to the Mott insulator transitions.

This work was supported by the National Natural Science Foundation of China (Nos. 12104433, 11874343) and the Innovation program for Quantum Science and Technology (No. 2021ZD0301200).

---

\* smhan@ustc.edu.cn

† helx@ustc.edu.cn

- [1] P. Anderson, Resonating valence bonds: A new kind of insulator?, *Materials Research Bulletin* **8**, 153 (1973).
- [2] P. W. Anderson, The resonating valence bond state in  $\text{La}_2\text{CuO}_4$  and superconductivity, *Science* **235**, 1196 (1987).
- [3] L. Balents, Spin liquids in frustrated magnets, *Nature* **464**, 199 (2010).
- [4] A. Kitaev, Fault-tolerant quantum computation by anyons, *Annals of Physics* **303**, 2 (2003).
- [5] A. Kitaev, Anyons in an exactly solved model and beyond, *Annals of Physics* **321**, 2 (2006), January Special Issue.
- [6] S. K. Choi, R. Coldea, A. N. Kolmogorov, T. Lancaster, I. I. Mazin, S. J. Blundell, P. G. Radaelli, Y. Singh, P. Gegenwart, K. R. Choi, S.-W. Cheong, P. J. Baker, C. Stock, and J. Taylor, Spin waves and revised crystal structure of honeycomb iridate  $\text{Na}_2\text{IrO}_3$ , *Phys. Rev. Lett.* **108**, 127204 (2012).
- [7] Y. Singh, S. Manni, J. Reuther, T. Berlijn, R. Thomale, W. Ku, S. Trebst, and P. Gegenwart, Relevance of the heisenberg-kitaev model for the honeycomb lattice iridates  $\text{A}_2\text{IrO}_3$ , *Phys. Rev. Lett.* **108**, 127203 (2012).
- [8] K. W. Plumb, J. P. Clancy, L. J. Sandilands, V. V. Shankar, Y. F. Hu, K. S. Burch, H.-Y. Kee, and Y.-J. Kim,  $\alpha$ - $\text{ruCl}_3$ : A spin-orbit assisted mott insulator on a honeycomb lattice, *Phys. Rev. B* **90**, 041112(R) (2014).
- [9] J. A. Sears, M. Songvilay, K. W. Plumb, J. P. Clancy, Y. Qiu, Y. Zhao, D. Parshall, and Y.-J. Kim, Magnetic order in  $\alpha$ - $\text{ruCl}_3$ : A honeycomb-lattice quantum magnet with strong spin-orbit coupling, *Phys. Rev. B* **91**, 144420 (2015).
- [10] S.-H. Baek, S.-H. Do, K.-Y. Choi, Y. S. Kwon, A. U. B. Wolter, S. Nishimoto, J. van den Brink, and B. Büchner, Evidence for a field-induced quantum spin liquid in  $\alpha$ - $\text{ruCl}_3$ , *Phys. Rev. Lett.* **119**, 037201 (2017).
- [11] A. U. B. Wolter, L. T. Corredor, L. Janssen, K. Nenkov, S. Schönecker, S.-H. Do, K.-Y. Choi, R. Albrecht, J. Hunger, T. Doert, M. Vojta, and B. Büchner, Field-induced quantum criticality in the kitaev system  $\alpha$ - $\text{ruCl}_3$ , *Phys. Rev. B* **96**, 041405(R) (2017).
- [12] J. A. Sears, Y. Zhao, Z. Xu, J. W. Lynn, and Y.-J. Kim, Phase diagram of  $\alpha$ - $\text{ruCl}_3$  in an in-plane magnetic field, *Phys. Rev. B* **95**, 180411(R) (2017).
- [13] S. Gass, P. M. Cónsoli, V. Kocsis, L. T. Corredor, P. Lampen-Kelley, D. G. Mandrus, S. E. Nagler, L. Janssen, M. Vojta, B. Büchner, and A. U. B. Wolter, Field-induced transitions in the kitaev material  $\alpha$ - $\text{ruCl}_3$  probed by thermal expansion and magnetostriction, *Phys. Rev. B* **101**, 245158 (2020).
- [14] S. Bachus, D. A. S. Kaib, Y. Tokiwa, A. Jesche, V. Tsurkan, A. Loidl, S. M. Winter, A. A. Tsirlin, R. Valentí, and P. Gegenwart, Thermodynamic perspective on field-induced behavior of  $\alpha$ - $\text{ruCl}_3$ , *Phys. Rev. Lett.* **125**, 097203 (2020).
- [15] S. Agrestini, C.-Y. Kuo, K.-T. Ko, Z. Hu, D. Kasinathan, H. B. Vasili, J. Herrero-Martin, S. M. Valvidares, E. Pellegrin, L.-Y. Jang, A. Henschel, M. Schmidt, A. Tanaka, and L. H. Tjeng, Electronically highly cubic conditions for ru in  $\alpha$ - $\text{ruCl}_3$ , *Phys. Rev. B* **96**, 161107(R) (2017).
- [16] J. c. v. Chaloupka, G. Jackeli, and G. Khaliullin, Kitaev-heisenberg model on a honeycomb lattice: Possible exotic phases in iridium oxides  $\text{A}_2\text{IrO}_3$ , *Phys. Rev. Lett.* **105**, 027204 (2010).
- [17] J. c. v. Chaloupka, G. Jackeli, and G. Khaliullin, Zigzag magnetic order in the iridium oxide  $\text{Na}_2\text{IrO}_3$ , *Phys. Rev. Lett.* **110**, 097204 (2013).
- [18] R. Schaffer, S. Bhattacharjee, and Y. B. Kim, Quantum phase transition in heisenberg-kitaev model, *Phys. Rev. B* **86**, 224417 (2012).
- [19] J. Reuther, R. Thomale, and S. Trebst, Finite-temperature phase diagram of the heisenberg-kitaev model, *Phys. Rev. B* **84**, 100406(R) (2011).
- [20] E. Sela, H.-C. Jiang, M. H. Gerlach, and S. Trebst, Order-by-disorder and spin-orbital liquids in a distorted heisenberg-kitaev model, *Phys. Rev. B* **90**, 035113 (2014).
- [21] X. Liu, T. Berlijn, W.-G. Yin, W. Ku, A. Tsvelik, Y.-J. Kim, H. Gretarsson, Y. Singh, P. Gegenwart, and J. P. Hill, Long-range magnetic ordering in  $\text{Na}_2\text{IrO}_3$ , *Phys. Rev. B* **83**, 220403(R) (2011).
- [22] F. Ye, S. Chi, H. Cao, B. C. Chakoumakos, J. A. Fernandez-Baca, R. Custelcean, T. F. Qi, O. B. Korneta, and G. Cao, Direct evidence of a zigzag spin-chain structure in the honeycomb lattice: A neutron and x-ray diffraction investigation of single-crystal  $\text{Na}_2\text{IrO}_3$ , *Phys. Rev. B* **85**, 180403(R) (2012).
- [23] S. R. Hassan, P. V. Sriluckshmy, S. K. Goyal, R. Shankar, and D. Sénéchal, Stable algebraic spin liquid in a hubbard model, *Phys. Rev. Lett.* **110**, 037201 (2013).
- [24] L. Liang, Z. Wang, and Y. Yu, Distinct-symmetry spin-liquid states and phase diagram of the kitaev-hubbard model, *Phys. Rev. B* **90**, 075119 (2014).
- [25] J. P. L. Faye, D. Sénéchal, and S. R. Hassan, Topological phases of the kitaev-hubbard model at half filling, *Phys. Rev. B* **89**, 115130 (2014).
- [26] A. Banerjee, C. A. Bridges, J.-Q. Yan, A. A. Aczel, L. Li, M. B. Stone, G. E. Granroth, M. D. Lumsden, Y. Yiu, J. Knolle, S. Bhattacharjee, D. L. Kovrizhin, R. Moessner, D. A. Tennant, D. G. Mandrus, and S. E. Nagler, Proximate kitaev quantum spin liquid behaviour in a honeycomb magnet, *Nature Materials* **15**, 733 (2016).
- [27] S. Mohapatra and A. Singh, Spin waves and stability of zigzag order in the hubbard model with spin-dependent hopping terms: Application to the honeycomb lattice

- compounds  $\text{Na}_2\text{IrO}_3$  and  $\alpha\text{-RuCl}_3$ , *Journal of Magnetism and Magnetic Materials* **479**, 229 (2019).
- [28] J. G. Rau, K.-H. Lee, and H.-Y. Kee, Generic spin model for the honeycomb iridates beyond the kitaev limit, *Phys. Rev. Lett.* **112**, 077204 (2014).
- [29] M. Lubasch, J. I. Cirac, and M.-C. Bañuls, Unifying projected entangled pair state contractions, *New Journal of Physics* **16**, 033014 (2014).
- [30] R. Orús, A practical introduction to tensor networks: Matrix product states and projected entangled pair states, *Annals of Physics* **349**, 117 (2014).
- [31] F. Verstraete, V. Murg, and J. Cirac, Matrix product states, projected entangled pair states, and variational renormalization group methods for quantum spin systems, *Advances in Physics* **57**, 143 (2008).
- [32] H. C. Jiang, Z. Y. Weng, and T. Xiang, Accurate determination of tensor network state of quantum lattice models in two dimensions, *Phys. Rev. Lett.* **101**, 090603 (2008).
- [33] F. Verstraete and J. I. Cirac, Renormalization algorithms for quantum-many body systems in two and higher dimensions, eprint arXiv:cond-mat/0407066 (2004).
- [34] W.-Y. Liu, S.-J. Dong, Y.-J. Han, G.-C. Guo, and L. He, Gradient optimization of finite projected entangled pair states, *Phys. Rev. B* **95**, 195154 (2017).
- [35] S.-J. Dong, C. Wang, Y. Han, G.-c. Guo, and L. He, Gradient optimization of fermionic projected entangled pair states on directed lattices, *Phys. Rev. B* **99**, 195153 (2019).
- [36] Z.-C. Gu, F. Verstraete, and X.-G. Wen, Grassmann tensor network states and its renormalization for strongly correlated fermionic and bosonic states, ArXiv e-prints (2010), arXiv:1004.2563 [cond-mat.str-el].
- [37] P. Corboz, R. Orús, B. Bauer, and G. Vidal, Simulation of strongly correlated fermions in two spatial dimensions with fermionic projected entangled-pair states, *Phys. Rev. B* **81**, 165104 (2010).
- [38] C. V. Kraus, N. Schuch, F. Verstraete, and J. I. Cirac, Fermionic projected entangled pair states, *Phys. Rev. A* **81**, 052338 (2010).
- [39] T. Barthel, C. Pineda, and J. Eisert, Contraction of fermionic operator circuits and the simulation of strongly correlated fermions, *Phys. Rev. A* **80**, 042333 (2009).
- [40] W.-Y. Liu, S. Dong, C. Wang, Y. Han, H. An, G.-C. Guo, and L. He, Gapless spin liquid ground state of the spin- $\frac{1}{2}$   $J_1 - J_2$  heisenberg model on square lattices, *Phys. Rev. B* **98**, 241109(R) (2018).
- [41] S. Okamoto, Global phase diagram of a doped kitaev-heisenberg model, *Phys. Rev. B* **87**, 064508 (2013).
- [42] R. Steinigeweg and W. Brenig, Energy dynamics in the heisenberg-kitaev spin chain, *Phys. Rev. B* **93**, 214425 (2016).
- [43] L. Janssen, E. C. Andrade, and M. Vojta, Honeycomb-lattice heisenberg-kitaev model in a magnetic field: Spin canting, metamagnetism, and vortex crystals, *Phys. Rev. Lett.* **117**, 277202 (2016).
- [44] M. Gohlke, R. Verresen, R. Moessner, and F. Pollmann, Dynamics of the kitaev-heisenberg model, *Phys. Rev. Lett.* **119**, 157203 (2017).
- [45] D. G. Joshi, Topological excitations in the ferromagnetic kitaev-heisenberg model, *Phys. Rev. B* **98**, 060405(R) (2018).
- [46] A. Metavitsiadis, C. Psaroudaki, and W. Brenig, Spin liquid fingerprints in the thermal transport of a kitaev-heisenberg ladder, *Phys. Rev. B* **99**, 205129 (2019).
- [47] P. M. Cönsoli, L. Janssen, M. Vojta, and E. C. Andrade, Heisenberg-kitaev model in a magnetic field:  $1/s$  expansion, *Phys. Rev. B* **102**, 155134 (2020).
- [48] K. Morita and T. Tohyama, Finite-temperature properties of the kitaev-heisenberg models on kagome and triangular lattices studied by improved finite-temperature lanczos methods, *Phys. Rev. Research* **2**, 013205 (2020).
- [49] S.-S. Zhang, G. B. Halász, W. Zhu, and C. D. Batista, Variational study of the kitaev-heisenberg-gamma model, *Phys. Rev. B* **104**, 014411 (2021).
- [50] E. Stoudenmire and S. R. White, Studying two-dimensional systems with the density matrix renormalization group, *Annual Review of Condensed Matter Physics* **3**, 111 (2012).